10-2009

Nonlinearity in Large Amplitude Oscillatory Shear (Laos) of Different Viscoelastic Materials

Xin Li

Shi-Qing Wang
University of Akron Main Campus, swang@uakron.edu

Xiaorong Wang

Nonlinearity in large amplitude oscillatory shear (LAOS) of different viscoelastic materials

Xin Li and Shi-Qing Wang[a)]

Department of Polymer Science, University of Akron, Akron, Ohio 44325

Xiaorong Wang

Bridgestone Americas, Center for Research and Technology, Akron, Ohio 44317

(Received 12 April 2009; final revision received 10 July 2009)

Synopsis

The present work investigates nonlinear behavior in large amplitude oscillatory shear (LAOS) of four different polymeric materials using simultaneous conventional rheometric measurements and particle-tracking velocimetric observations. In contrast to most studies in the literature that treat nonlinearity in LAOS in steady state, we emphasize by the present four examples that nonlinearity in LAOS often arise in complex fluids due to time-dependent rearrangement of their microstructures in response to LAOS. Consequently, no correlation is obvious between strain dependence of the steady-state stress response and the time-dependent characteristics of the steady-state response. For instance, a highly viscoelastic material made of nano-sized polybutadiene particles exhibits homogeneous deformation and an approximate sinusoidal wave despite strong strain softening. In a second example, a well-entangled polybutadiene solution becomes inhomogeneous over time, and the corresponding nonlinearity (i.e., strain softening) took a finite time to develop to its fullest. In the example of wall slip of a monodisperse entangled polyisoprene melt, contrary to the literature claim that *even* harmonics would emerge, we show that the stress response only involves odd harmonics in the absence of any edge fracture. Last, a polydisperse poly(dimethyl siloxane) melt experiences homogeneous LAOS without displaying significant higher harmonics in the absence of any edge failure. In contrast, the Fourier transform analysis shows that meniscus failure is responsible for the emergence of higher harmonics including some *even* ones. © *2009 The Society of Rheology.* [DOI: 10.1122/1.3193713]

I. INTRODUCTION

Many structured materials, either biological or synthetic, including colloids, polymers, liquid crystals, micelles, foams, gels (e.g., associating polymers, ionomers, gelatins, etc.), emulsions and membranes, exhibit viscoelastic behavior due to the microscopic organization of the constituents into cooperative structures. Characteristics of the microstructure dictate its viscoelastic responses and determine when and how nonlinearity may arise. For example, polymeric liquids derive their structure from chain entanglement, i.e., the inability for chain-like molecules to freely pass across one another within their overall relaxation time τ. Upon a sudden startup shear at a rate $\dot{\gamma}$ corresponding to the Weissen-

[a)]Author to whom correspondence should be addressed; electronic mail: swang@uakron.edu

berg number $\mathrm{Wi} = \dot{\gamma}\,\tau \gg 1$, chains in a well-entangled polymer are forced to pass around one another without waiting for thermal diffusion to move them past, at which point the initial elastic deformation transforms to viscous flow [Wang and Wang (2009)].

Linear viscoelasticity is both conceptually and technically more straightforward to characterize. One aspect of nonlinearity arises from the large amplitude oscillatory shear (LAOS). The present work focuses on a generic study of nonlinearity in the stress response to LAOS, i.e., an externally imposed oscillatory shear strain $\gamma = \gamma_0 \sin \omega t$. For many viscoelastic materials, the shear stress $\sigma(t;\omega,\gamma_0)$ is not linearly proportional in magnitude to γ_0 when γ_0 exceeds a critical value γ_c. In the literature, nonlinear responses to LAOS are typically studied under the condition of steady state and homogeneous deformation [Tee and Dealy (1975); Giacomin and Oakley (1992); Reimers and Dealy (1996); Wilhelm (2002); Cho *et al.* (2005); Klein *et al.* (2007); Jeyaseelan and Giacomin (2008); Ewoldt *et al.* (2008); Yu *et al.* (2009)], where $\sigma^{ss}(t;\omega,\gamma_0)$ is a periodic function of time. In this case, the final steady-state response can be represented completely by a Fourier series,

$$\sigma^{ss}(t;\omega,\gamma_0) = \sum_{n=1}^{\infty} [a_n(\omega,\gamma_0)\sin(n\omega t) + b_n(\omega,\gamma_0)\cos(n\omega t)], \tag{1}$$

where a_n and b_n represent, respectively, the elastic and viscous-like components of the stress responses. In terms of the generalized storage and loss moduli G_n' and G_n'', the coefficients $a_n = \gamma_0 G_n'$ and $b_n = \gamma_0 G_n''$ by definition. A Fourier transform (FT) analysis can be made of $\sigma^{ss}(t;\omega,\gamma_0)$ to determine all of $\{G_n'\}$ and $\{G_n''\}$ for all values of ω and γ_0. Wilhelm and co-workers (1998; 1999) advocated this FT rheology method. In the case where the stress response is of odd symmetry with respect to the directionality of shear strain and shear rate, i.e., when the material response is the same upon reversal of shear and n is odd in the Fourier series of Eq. (1), Cho *et al.* (2005) avoided performing a FT rheology analysis by decomposing the stress response into elastic and viscous components. Two recent studies further discussed alternative methods to the FT analysis [Ewoldt *et al.* (2008); Yu *et al.* (2009)], where the goal is to find a more definitive way to quantify the steady-state stress response, although the convergence of the Fourier series of Eq. (1) is typically rather rapid. Since the time and strain dependence of $\sigma^{ss}(t;\omega,\gamma_0)$ does not usually depict how the system evolves over time from its equilibrium state to the final non-equilibrium steady state, mathematical features of $\sigma^{ss}(t;\omega,\gamma_0)$ can hardly be regarded as the full rheological fingerprint. Besides, these theoretical analyses presume homogeneous deformation prevails during LAOS and cannot apply to any situation where the sample does not suffer uniform amplitude of oscillatory shear.

It is our view that many, perhaps, most viscoelastic systems respond to LAOS in a time-dependent fashion, including particle-filled polybutadiene (PBD) melts [Zhu *et al.* (2005)] and entangled PBD solutions [Ravindranath and Wang (2008a)]. The purpose of this work is to describe four more examples where strain softening occurs as a result of structural yielding over time. These four systems have been selected to illustrate how yielding behavior is different, from a polymeric nano-granular paste, to an entangled melts of linear chains with either broad or narrow molecular weight distribution, and to an entangled polymer solution. With the assistance of particle-tracking velocimetry (PTV) [Wang (2007)], we have identified the following four characteristics accompanying the LAOS: (i) homogeneous strain softening of a polymeric paste, (ii) shear banding of an entangled polymer solution, (iii) interfacial wall slip of one polymer melt, and (iv)

homogenous yielding of a polydisperse melt. It is clear that a full characterization of nonlinearity in LAOS requires us to pay more attention to the structural transformation over time.

II. EXPERIMENTAL

A. Materials

Four materials are studied in this work. (A) The first sample is a highly viscoelastic material made of nano-sized spherical PBD particles. The nanoparticle has a crosslinked polystyrene core and a shell of PBD brushes (with 8.4% vinyl content, 45.6% cis, and 46.0% trans). The average size of the nanoparticle is around 9 nm, and the core/shell ratio is around 1/4. The polydispersity of these particles is around 1.15. The PBD brush molecular weight is around 15 kg/mol, and the average number of PBD chains per particle is around 27. More details about this material can be found in the literature [Wang *et al.* (2007)]. (B) The second sample is an entangled solution at a concentration of 10% high molecular-weight monodisperse 1,4-PBD (M_w=1100 kg/mol, 1,4-addition >90%, $T_g \sim -100$ °C) in an oligomeric monodisperse PBD (M_w=10 kg/mol, 1,4-addition >90%, $T_g \sim -100$ °C). The sample was prepared by first dissolving PBD 1 M in toluene and then mixing with PBD 10 K. Toluene was then allowed to evaporate from the uniform solution at room temperature for a week under a hood. The residual toluene was completely removed under vacuum for about 3 days. (C) The third sample under present study is a monodisperse 1,4-polyisoprene (PI) melt made by Goodyear Tire and Rubber company with the following characteristics: cis-1,4 (75.0%), trans-1,4 (16.4%), and −3.4 (6.6%), M_w=547 K (g/mol), and M_n=516 K (g/mol). (D) The last sample is a polydisperse poly(dimethyl siloxane) (PDMS) melt from GE Silicones (product No: SE54) with M_z=1479 kg/mol, M_w=878.2 kg/mol, and M_n=538.6 kg/mol.

B. PTV

Interpretation of most previous rheometric studies is predicated on the assumption that homogeneous deformation prevails during measurements. It should now be common knowledge that for complex fluids, such as the four polymeric liquids under study, the validity of the homogeneous-shear assumption must always be verified. PTV [Wang (2007)] has been effectively applied since 2006 [Tapadia and Wang (2006)] to complement traditional rheometric experiments on entangled polymeric liquids, ranging from sudden startup shear [Tapadia and Wang (2006); Boukany and Wang (2007); Ravindranath and Wang (2008b)], LAOS [Tapadia *et al.* (2006); Ravindranath and Wang (2008a)], and large step shear [Wang *et al.* (2006); Ravindranath and Wang (2007); Boukany, Wang, and Wang (2009)].

A PTV setup is also indispensable in the present work. By sending a laser sheet across the sample thickness to illuminate particles embedded in the sample, we can measure the time-dependent deformation field with video microscopy. For the purpose of PTV observations, we have incorporated about 600 ppm silver-coated particles with an average diameter of 10 μm (Dantec Dynamics HGS-10) into each of the four samples. Since depiction of a PTV apparatus has been published previously [Tapadia and Wang (2006); Ravindranath and Wang (2008b)], we omit an explicit graphic illustration.

C. Apparatus

All measurements were made with an advanced expansion rheometric system (ARES), equipped with different customer-made fixtures. Measurements of PI 550 K and PDMS

were performed with a 4° cone-plate fixture with diameter of 10 and 15 mm, respectively. Wall slip behavior of PI 550 K is observed directly at the meniscus. The experiments on nano-PBD-particle paste were carried out in a partitioned-plate-cone device that has been described previously [Ravindranath and Wang (2008b)]. In the partitioned-plate-cone device setup, the bottom rotating cone-plate has a 4° angle and a diameter of 30 mm. As part of the top surface, an inner circular disk of 15 mm in diameter is linked to the torque transducer of ARES. The top outer ring is held fixed and has a gap around 0.2 mm with the inner circular disk. The ring's outer diameter matches that of the bottom cone equal to 30 mm. This partitioned-plate-cone apparatus was also used to eliminate edge effects for PI and PDMS melts. Finally, the entangled 1 M-10%-10 K solution was studied with a cone-plate with a diameter of 25 mm and 4° cone angle. It is worth mentioning that at moderate angular frequencies employed in the present study, ARES is capable of delivering nearly perfect sine wave even in much of the initial cycle in the *arbitrary wave* mode. All measurements were carried out at room temperature around 24 °C.

D. FT analysis

When steady state is achieved, the stress response to $\gamma = \gamma_0 \sin \omega t$ is a periodic function of time and can be expressed as a Fourier series as shown in Eq. (1). The amplitudes $\{a_n, b_n\}$ of each term from the fundamental harmonic to other harmonics in Eq. (1) can be evaluated according to

$$a_n(\omega, \gamma_0) = \frac{2}{T}\int_{-T/2}^{T/2} \sigma(t; \omega, \gamma_0) \sin n\omega t dt, \tag{2a}$$

and

$$b_n(\omega, \gamma_0) = \frac{2}{T}\int_{-T/2}^{T/2} \sigma(t; \omega, \gamma_0) \cos n\omega t dt, \tag{2b}$$

where T is the period of the LAOS equal to $2\pi/\omega$. The intensity of the various harmonic waves is defined by

$$I_n(\omega) = [(a_n)^2 + (b_n)^2]^{1/2}. \tag{3}$$

Thus, any given periodic stress response of Eq. (1) can be expressed in terms of a normalized power spectrum of $I(\varpi)/I_1(\omega)$, where $I(\varpi)$ is evaluated according to Eqs. (2) and (3) with $n\omega$ replaced by ϖ. In our FT analysis, we typically evaluate I_n over several cycles to reduce the noise level.

E. Data representation

ARES not only outputs in its software data on G_1' and G_1'' during LAOS but also exports the actual data of the time-dependent torque and angular displacement, respectively. The transient raw data can be captured using a digital reading card DATAQ DI-154RS with a rate of 30 data points per second when the fundamental frequency is 0.5 and 1 rad/s. For the LAOS frequency equal to 5 rad/s, the data collection rate can be set to 120/s. The stress power spectra are calculated by performing FT on an average of five cycles. When instructive, we also present how the peak stress value σ_{peak} changes with time during LAOS.

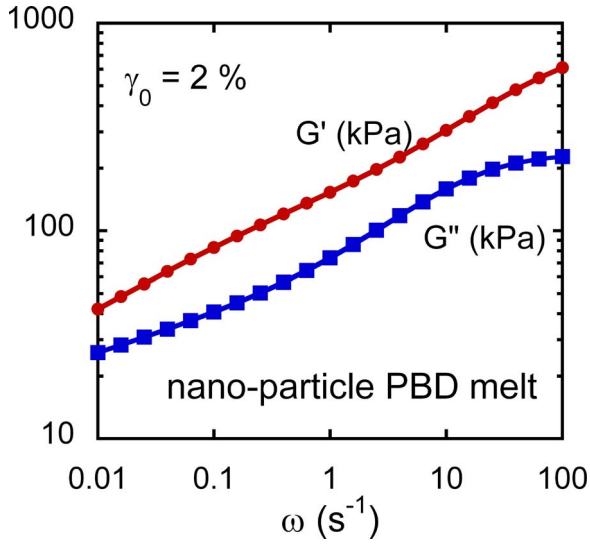

FIG. 1. Dynamic and loss moduli G' and G'' from SAOS measurements at γ_0=2% of the nano-granular PBD melt.

III. RESULTS AND DISCUSSION

A. Homogeneous yielding of nano-granular paste of PBD particles

Any LAOS study of an unknown system may begin with a small amplitude oscillatory shear (SAOS) frequency sweep. Figure 1 shows the SAOS data at a strain of 2%. Figure 2 shows the FT analysis of the SAOS stress signal at γ_0=5% and ω=1 rad/s, along with a steady-state Lissajous plot (shear stress vs shear strain loop) in the inset. At such low strains, the Lissajous plot is perfectly elliptical and harmonics are negligibly small. Moreover, characteristic of linear response behavior, the peak stress σ_{peak} is found to be

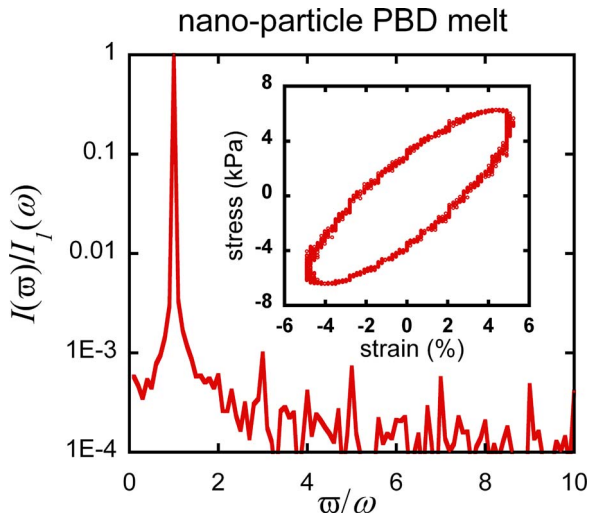

FIG. 2. FT analysis of the shear stress and stress-strain loop of the nano-granular PBD melt at γ_0=5% and ω=1 rad/s.

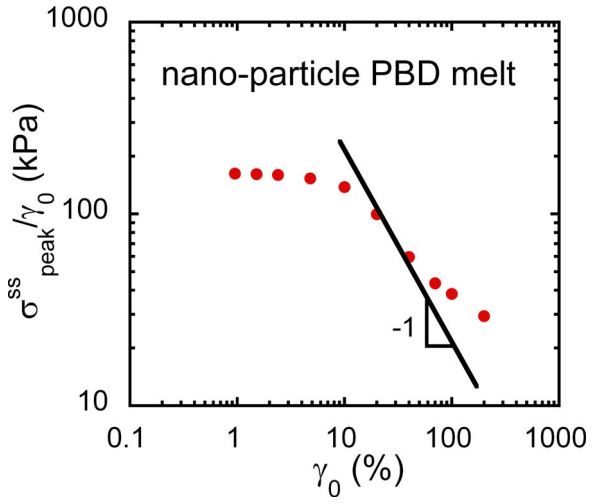

FIG. 3. Strain softening expressed in terms of the steady-state "complex modulus" $\sigma^{ss}_{peak}/\gamma_0$ as a function of the amplitude γ_0.

constant in time. The gel-like rheological characteristic is indicative of close-packing of the nano-sized PBD particles that leads to jamming and inability of the paste to display terminal flow behavior on a reasonable experimental time scale.

When γ_0 is higher than around 20%, σ_{peak} becomes time dependent and is no longer linearly proportional to γ_0. In steady state, the strain softening can be expressed as shown in Fig. 3, where the slope of -1 is merely to indicate the limit of maximal strain softening. Over a range from $\gamma=10\%$ to 40%, the magnitude of the complex modulus $\sigma^{ss}_{peak}/\gamma_0$ actually decreases by a factor of nearly 3 at $\gamma_0=40\%$ from its value in the linear response ($\gamma_0<10\%$) regime.

The emergence of the harmonic at 3ω also occurs around $\gamma_0=20\%$. For example, at $\gamma_0=40\%$, the stress response (peak stress σ_{peak}) declines in magnitude over time, and G_1' drops below G_1'' after 200 s, as shown in Fig. 4(a). In the steady state, intriguingly enough, the stress signal is almost completely sinusoidal, with the Lissajous plot looking like a decent ellipse in the inset of Fig. 4(b) although the FT analysis detects a small amount of harmonics, as shown in Fig. 4(b). Since the intensity of the third harmonic is only as low as 3% that of the base harmonic, the steady-state stress σ^{ss} can be approximately written as

$$\sigma^{ss}(t;\omega,\gamma_0)=\sigma^{ss}_{peak}(\gamma_0)\sin(\omega t+\delta). \tag{4}$$

The approximate sinusoidal character of Fig. 4(b) expressed in Eq. (4) obviously does not capture the strong strain softening depicted by $\sigma^{ss}_{peak}(\gamma_0)$ in Fig. 3. To better comprehend the strain softening phenomenon, it is instructive to examine at a high strain γ_0 how the system initially responds to the imposed LAOS that is realized in the arbitrary wave mode in ARES. Figure 5(a) shows how the Lissajous loops evolve in time under the condition of $\gamma_0=70\%$, $\omega=1$ rad/s. Clearly, the equilibrium state has yielded to the LAOS and is developing toward a new softer microstructure over time. This process can be more clearly delineated by examining the raw stress data of strain and stress for the first five cycles in Fig. 5(b): the peak shear stress (blue dots) drops over time. Eventually, the system arrives at a new state capable of approximate sinusoidal response to the imposed LAOS. This is possible if the new steady state under the LAOS does not

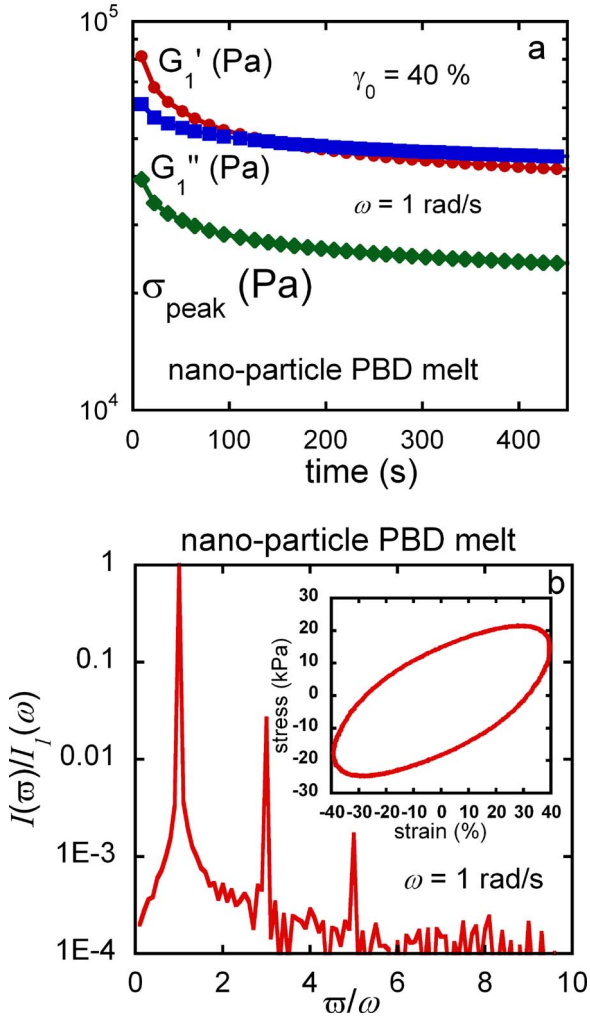

FIG. 4. (a) Decline of the storage and loss moduli corresponding to the first harmonic as well as the peak value of the shear stress as a function of time for γ_0=40% and ω=1 rad/s. (b) FT analysis of the stress response in steady state for γ_0=40% and ω=1 rad/s, in terms of the normalized power spectrum, where the inset shows the Lissajous plot.

undergo further structural change within each cycle. This new state plausibly corresponds to packing of the nano-particles into layers that are long lived, i.e., stable during the LAOS.

Since the nano-particle paste is free of chain entanglement, we do not expect the yielding to occur inhomogeneously. Our PTV observations indeed confirm the occurrence of uniform straining during the LAOS at all moments within each cycle. Figure 5(c) shows a linearly varying velocity field in steady state at the moment when the driving surface attains the maximum speed. Thus, the present nano-granular paste of PBD particles offers an example of homogeneous yielding during LAOS. To reiterate, the absence of chain entanglement ensures that no structural failure through the packing rearrangement would result in any drastic reduction of the local shear viscosity. Consequently, the structure change during yielding was able to proceed homogeneously.

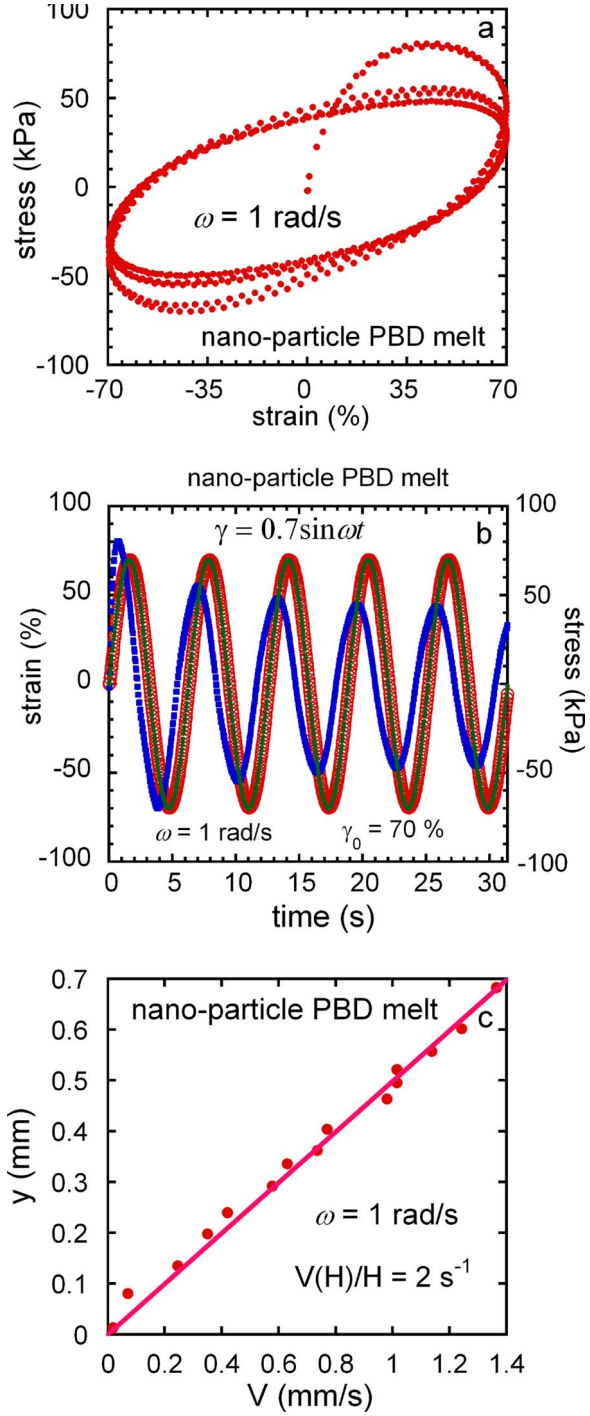

FIG. 5. LAOS at γ_0=200%, ω=1 rad/s: (a) stress-strain loop of the first three cycles; (b) explicit raw data of strain and stress in the first five cycles; and (c) PTV observations confirming homogeneous LAOS.

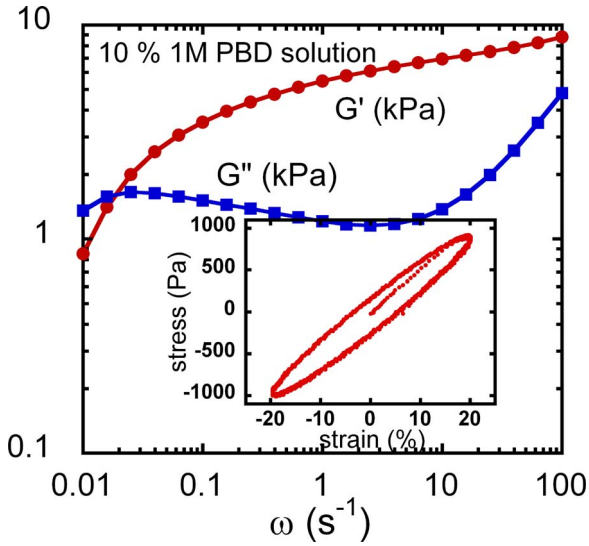

FIG. 6. Dynamic and loss moduli G' and G'' from SAOS measurements at $\gamma_0=5\%$ of the 10% 1 M PBD solution, where the inset shows an elliptical Lissajous loop for $\gamma_0=20\%$.

B. Shear banding in entangled PBD solutions

Shear banding has been reported for highly entangled polymer solutions during LAOS [Ravindranath and Wang (2008a)]. Figure 6 presents the SAOS frequency sweep measurement, showing the crossover frequency $\omega_c=\tau^{-1}$ to be around 0.02 rad/s. The oscillatory shear at $\gamma_0=20\%$ is SAOS because the stress-strain loops of the first three cycles show closed elliptical loops in the inset of Fig. 6, rather different from those observed for LAOS in Fig. 8(b) below. In the present study, we choose to perform LAOS at $\omega=1$ rad/s, corresponding to a Deborah number $\omega\tau$ of 50.

For γ_0 between 0 and 70%, we only observe linear response—the stress peak does not decline over time, and time dependence is an ideal sinusoidal wave. FT analysis in the inset of Fig. 7 further illustrates the absence of harmonics in the linear response regime, e.g., at $\gamma_0=10\%$. Apparent strain softening occurs at higher amplitudes. Actually, the stress response is almost ideal yield-like beyond 70% as shown in Fig. 7—the slope of -1 amounts to having $\sigma^{ss}_{peak}=$const.

In LAOS, e.g., at $\gamma_0=200\%$, $\omega=1$ rad/s, Fig. 8(a) shows the decline of σ_{peak}, G_1', and G_1'', respectively. Figure 8(b) of stress vs strain loops for the first three cycles illustrates yielding behavior. The sample first elastically deforms in response to the strain of $\gamma=\gamma_0 \sin \omega t$, with the shear stress σ growing monotonically. At $\gamma=160\%$, yielding occurs as the shear stress starts to drop. This is analogous to stress overshoot or yielding during startup deformation at a high deformation rate [Wang and Wang (2009)] because the shear stress does not return to the initial level in the subsequent cycles, strongly indicative of structural changes in the sample.

We carry out PTV observations, following the yielding process. It is worth mentioning that the deformation field is homogeneous in the first several cycles. After five cycles, shear banding emerges as the stress response drops further according to Fig. 8(a). Figure 8(c) shows how the velocity profile changes in steady state when the shear banding is strongest. In each cycle, the apparent shear rate is continuously changing from 0 to $\gamma_0\omega$ and moments at A and C are equivalent and so are points B and D as indicated in Fig.

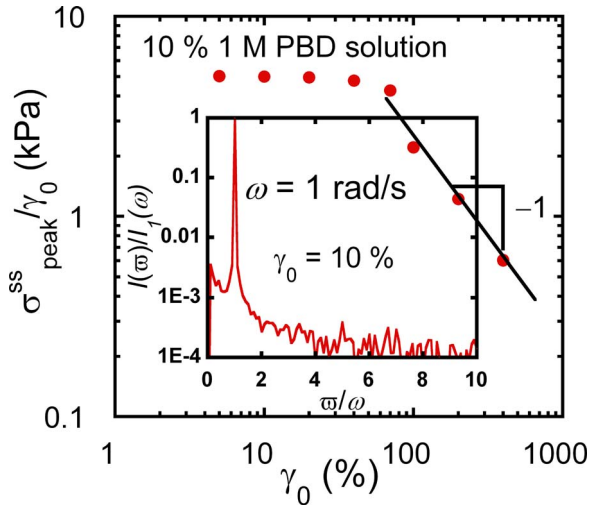

FIG. 7. Strain softening expressed in terms of the steady-state complex modulus $\sigma^{ss}_{peak}/\gamma_0$ as a function of the amplitude γ_0, where the FT analysis in the inset shows an ideal sinusoidal stress response at a low strain.

8(c). Apparently, inhomogeneous yielding occurs between A and B (or C and D) so that strong shear banding is present at both B and D. When the driving shear rate diminishes toward zero, the system heals from its "wound," and the healed sample exhibits homogeneous shear again at moments A and C as confirmed by the PTV observations. Thus,

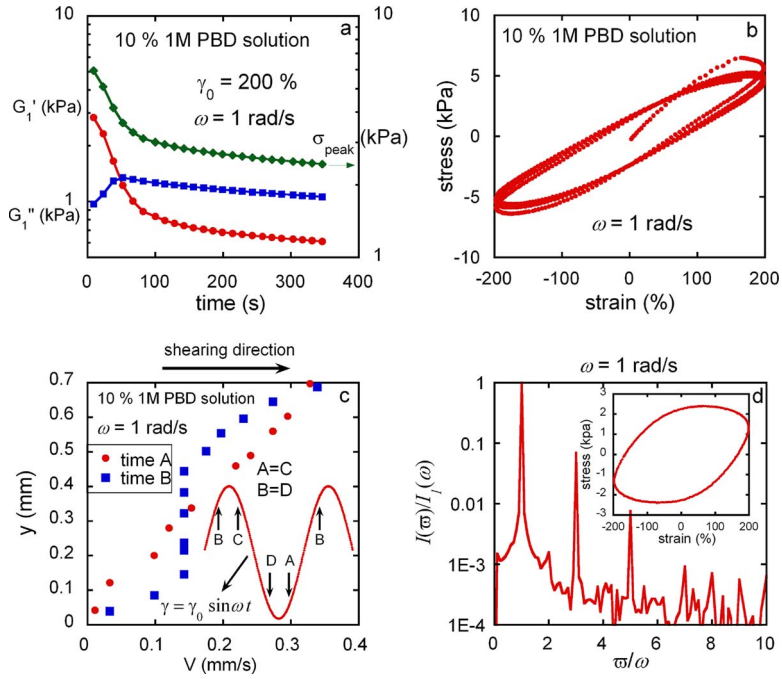

FIG. 8. LAOS of the of 10 % 1 M PBD solution at γ_0=200% and ω=1 rad/s: (a) time dependence of σ_{peak} and G_1' and G_1''; (b) stress-strain loops of the first three cycles; (c) PTV measurements of the velocity profiles at two different moments in a steady-state cycle, where the moments of A and C are equivalent, so are moments B and D; and (d) FT analysis of the raw shear stress data along with the Lissajous plot.

although at times A and B the apparent transient strain and shear rate are, respectively, of the same magnitude the deformation field is completely different. Clearly, the system is unable to settle down to a single state of entanglement within each cycle, even in steady state. This is the origin of strong non-sinusoidal response of the shear stress. Figure 8(d) indicates that the stress response contains considerable harmonics as disclosed by the FT analysis as well as the non-elliptical shape of the Lissajous plot.

Entangled polymers, such as the present 10% solution, are a primary example for nonlinearity in LAOS, where the structural change occurs even in a steady state within each cycle to produce the significant non-sinusoidal responses. They also display strain softening in the traditional sense as illustrated in Fig. 7.

C. Wall slip of a well-entangled PI melt

1. Wall slip and edge fracture

For well-entangled melts of linear chains, wall slip is often observed at high shear stresses or strains [Brochard and de Gennes (1992); Wang (1999)]. Boukany and Wang (2009) recently described how interfacial yielding arises during startup shear as a result of chain disentanglement. Under LAOS, Hatzikiriakos and Dealy (1991), Adrian and Giacomin (1992), and Reimers and Dealy (1996) observed even harmonics. It was unclear whether wall slip produces the observed asymmetric stress response within each cycle. On the other hand, Hatzikiriakos and Dealy (1991) used a Maxwell-like time-dependent model for wall slip to produce similar stress responses as observed in their experiment, implying that wall slip played a role in creating the observed wave distortions. Another theoretical study based on a memory-slip model [Graham (1995)] also concluded that wall slip would allow even harmonics to emerge along with odd harmonics in the shear stress response. It has also been speculated that even harmonics would occur in certain constitutive models in the absence of wall slip [Atalik and Keunings (2004)]. It is thus interesting and important to determine by experiment not by modeling the various characteristics of LAOS of polymer melts when wall slip is the dominant response and other factors are unimportant.

First, a SAOS measurement is carried out to show in Fig. 9(a) that the terminal relaxation time τ is approximately 54 s. In the linear response regime, Fig. 9(b) reveals completely sinusoidal stress response, where the corresponding Lissajous plot is perfectly elliptical. When $\gamma_0 > 40\%$ with $\omega = 0.5$ rad/s, PI 550 K starts to show wall slip and the stress response is strongly nonlinear. Figure 10(a) shows the time dependence of σ_{peak}, G_1', and G_1'' at $\gamma_0 = 70\%$ and $\omega = 0.5$ rad/s, where the dashed line indicates the stress response in the absence of any edge failure, which is a condition to be discussed in detail below. At around $t = 300$ s, the stress response, characterized by the FT analysis in Fig. 10(b), shows the emergence of even harmonics as well as a strongly non-elliptical Lissajous plot. A careful inspection of the Lissajous loop indicates a slight loss of a rotational symmetry about the origin, consistent with the appearance of *even* harmonics.

By measuring movements of particles on the meniscus, we obtain the signature of wall slip in Fig. 10(c) during the LAOS at $\gamma_0 = 70\%$ and $\omega = 0.5$ rad/s. Analogous to Fig. 8(c), severe yielding occurs at both interfaces at B or D. No-slip boundary condition is recovered at A and C when the instantaneous shear rate diminishes to allow healing of the interface through chain re-entanglement. The video microscopy on the edge also reveals meniscus failure.

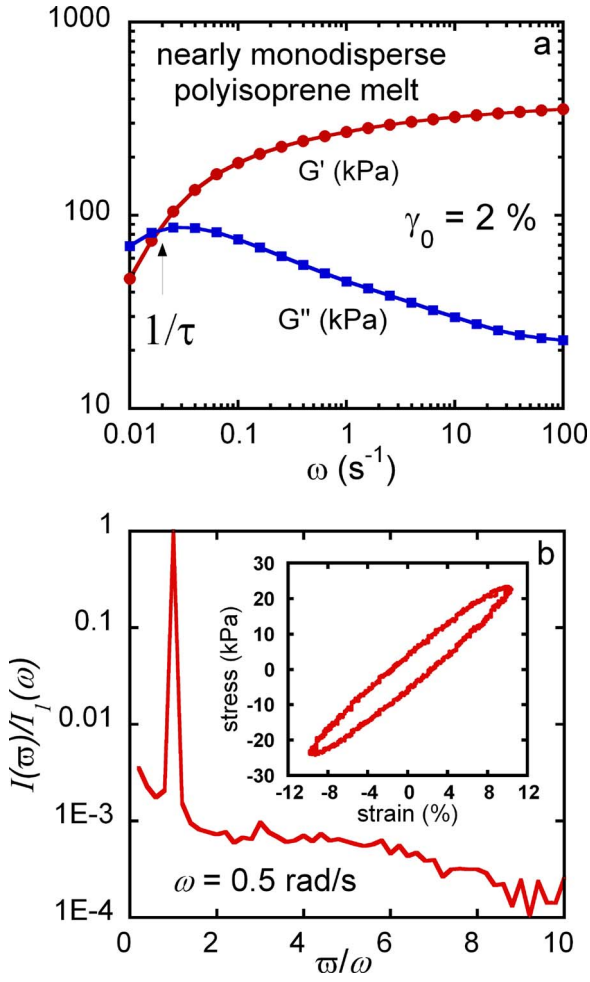

FIG. 9. (a) Dynamic and loss moduli G' and G'' from SAOS measurements at γ_0=2% of the PI melt. (b) FT analysis of the shear stress and stress-strain loop of the PI melt at γ_0=10% and ω=0.5 rad/s.

2. Absence of even harmonics in wall slip

To remove any influence of edge fracture on the LAOS characteristics during wall slip, we have adopted a literature design [Ravindranath and Wang (2008b)] to decouple the rheometric measurements from the edge instability. Using such a partitioned-plate-cone setup, we find that the shear stress quickly stabilizes to its steady state as shown in Fig. 11(a) in contrast to Fig. 10(a). Contrary to all the other three systems studied in this work, G_1' stays above G_1'' in steady state. Because of the interfacial slip, the imposed LAOS cannot be effectively applied to the bulk of the sample, so that the bulk still deforms in the linear response regime. In other words, the bulk sample does not get transformed into a liquid and remains well entangled and solid-like on the time scale of the LAOS experiment, consistent with the fact that $G_1' > G_1''$. Equally interesting and important is the FT analysis of the rheometric measurements that discloses only odd harmonics in Fig. 11(b), contrary to the result of Fig. 10(b), implying that the emergence of even harmonics is due to edge effects. In other words, true wall slip in LAOS appears free of even harmonics, in odds with the previous conclusions due to [Hatzikiriakos and

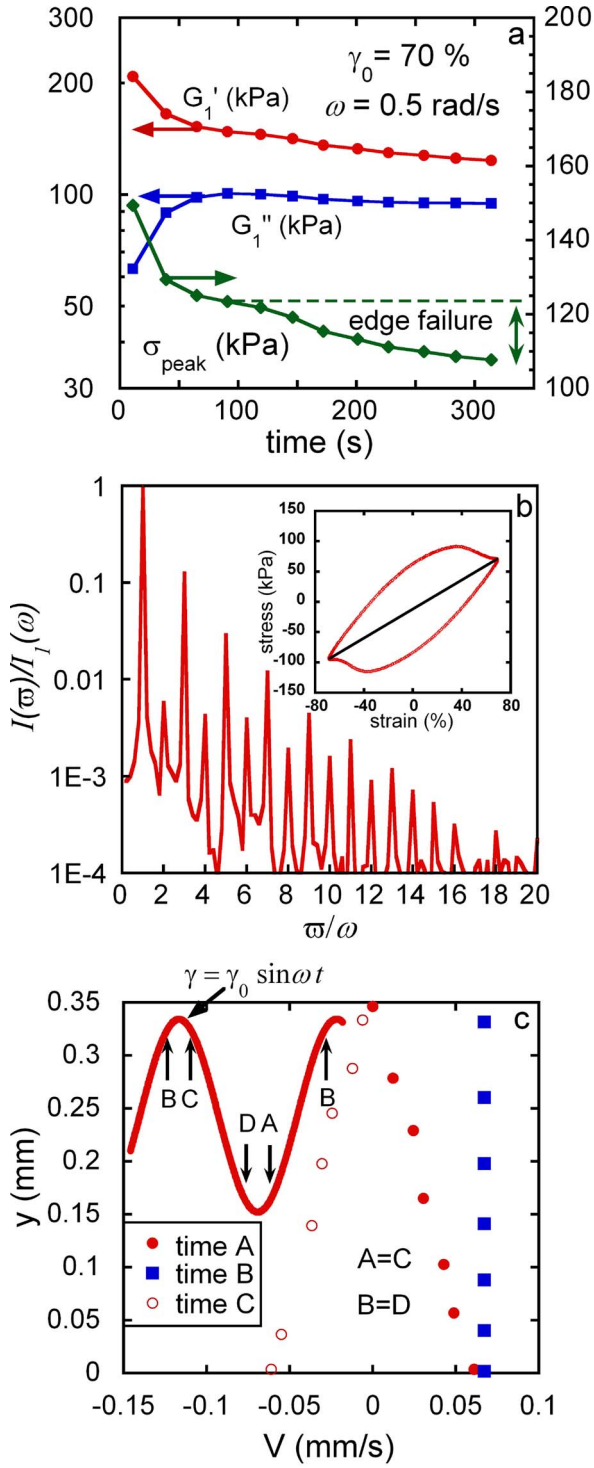

FIG. 10. (a) Time dependence of σ_{peak}, G_1', and G_1'' at γ_0=70% and ω=0.5 rad/s, where the horizontal dashed line is "borrowed" from Fig. 11. (b) FT analysis of the shear stress at around t=300 s, showing an emergence of even harmonics as well as a strongly non-elliptical Lissajous plot in the inset. (c) PTV measurements of the velocity profiles at three moments in a steady-state cycle, where the moments of A and C are equivalent, so are moments B and D.

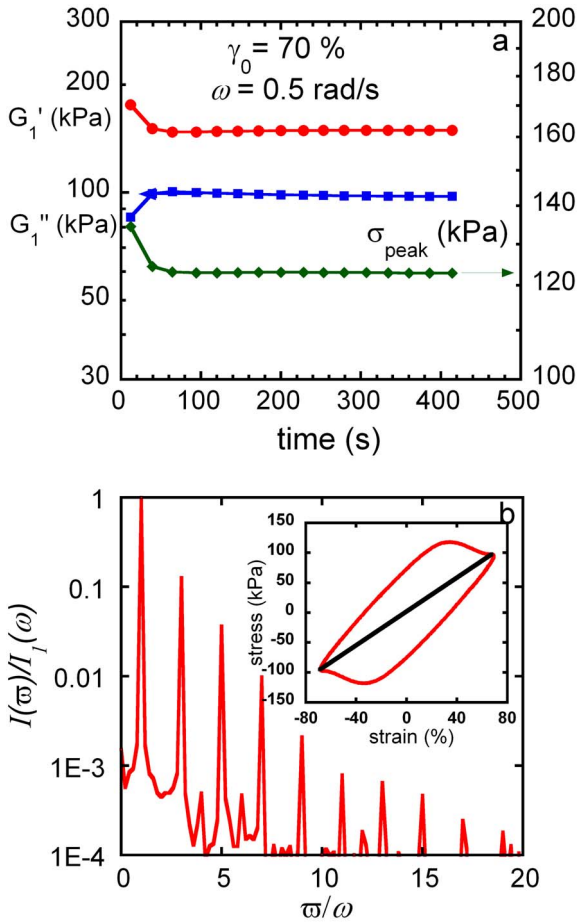

FIG. 11. (a) Time dependence of σ_{peak}, G_1', and G_1'' at γ_0=70% and ω=0.5 rad/s measured with the partitioned-plate-cone device [Ravindranath and Wang (2008b)]. (b) FT analysis of the shear stress at any time after t =100 s, with a Lissajous loop that is more symmetric than that in the inset of Fig. 10(b).

Dealy (1991); Adriana and Giacomin (1992); Graham (1995); Ewoldt *et al.* (2008)]. On the other hand, we did not rule out that wall slip cannot produce even harmonics.

Emergence of strong harmonics is evident from Fig. 11(b) even in the absence of edge failure in this example of wall slip because the system alternates between slip and no-slip within each cycle, i.e., the state of deformation is oscillating instead of stationary. Thus, wall slip in LAOS joins the example of LAOS banding of entangled polymer solutions as a case where severe nonlinear character in steady state originates from the ability of the system to respond differently during the different moments within each cycle, i.e., wall slip at B and to no-slip at C.

D. LAOS of a polydisperse PDMS melt

1. Characteristics of LAOS due to edge fracture

Finally, we use a polydisperse PDMS to depict how edge failure produces wave distortion in LAOS in the absence of interfacial wall slip. The SAOS in Fig. 12 confirms that PDMS has a broad molecular weight distribution. Figure 13(a) shows the time

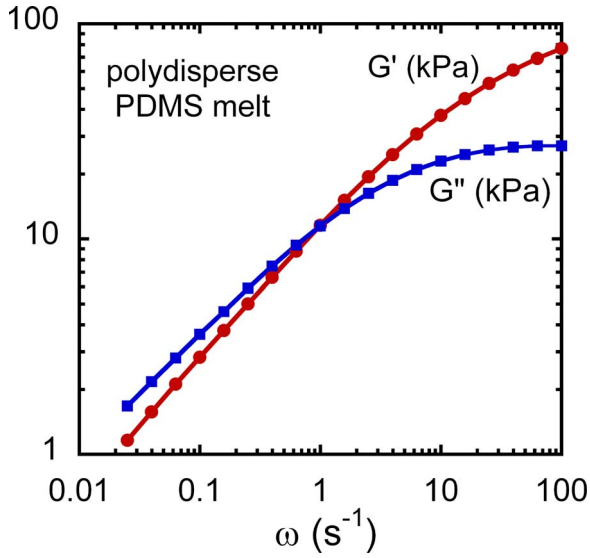

FIG. 12. Dynamic and loss moduli G' and G'' from SAOS measurements at $\gamma_0=5\%$ of the PDMS melt.

dependence of the stress response at both low strain $\gamma_0=10\%$ and high strain $\gamma_0=200\%$ at $\omega=5$ rad/s. The PDMS melt shows linear response behavior at $\gamma_0=10\%$. However, at $\gamma_0=200\%$, G_1' falls below G_1'' immediately, and both G_1' and G_1'' decrease further over time. For example, around $t=37$ s, the stress-strain loops in the inset of Fig. 13(b) depict the evolution of the stress response whose FT analysis reveals a number of odd harmonics. In a quasi-steady state around $t=120$ s, small even harmonics along with additional odd harmonics are also visible from the FT analysis in Fig. 13(c). A visual inspection of the meniscus shows that the edge integrity could not be maintained during the LAOS. In a traditional cone-plate setup, the occurrence of edge fracture makes the LAOS rheometric measurements of polymer melts unreliable. The strong wave distortion of the stress response and decline of the shear stress may have stemmed from the edge failure that causes the effective amount of sample under LAOS to decrease in time.

2. Characteristics of LAOS in absence of edge fracture

To separate the experimental complication of edge effects from the true and intrinsic rheological response of the polydisperse PDMS melt under LAOS, we again adopt the partitioned-plate-cone setup of Ravindranath and Wang (2008b). This effective apparatus allows us to demonstrate in Fig. 14(a) that nearly all the time-dependent drop of the shear stress observed in Fig. 13(a) was due to the deterioration of edge integrity. In other words, in the absence of the edge effects, the PDMS melt quickly attains stable LAOS behavior with G_1' below G_1''. Upon FT analysis of the shear stress data, we confirm that in the absence of the edge effects the steady-state stress response does not deviate significantly from a sinusoidal wave depicted by Eq. (4). There is only a fairly weak third harmonic term in Fig. 14(b), where the inset shows a very slightly distorted elliptical Lissajous loop. Furthermore, PTV observations indicate that the LAOS is homogeneous. Thus, this is an example analogous to the nano-granular PBD melt, where the nonlinearity of LAOS is not accompanied by shear banding or interfacial failure, and the stress response is nearly sinusoidal. The PDMS is highly polydisperse as evident from the SAOS data of Fig. 12. The broad molecular weight distribution in the present PDMS

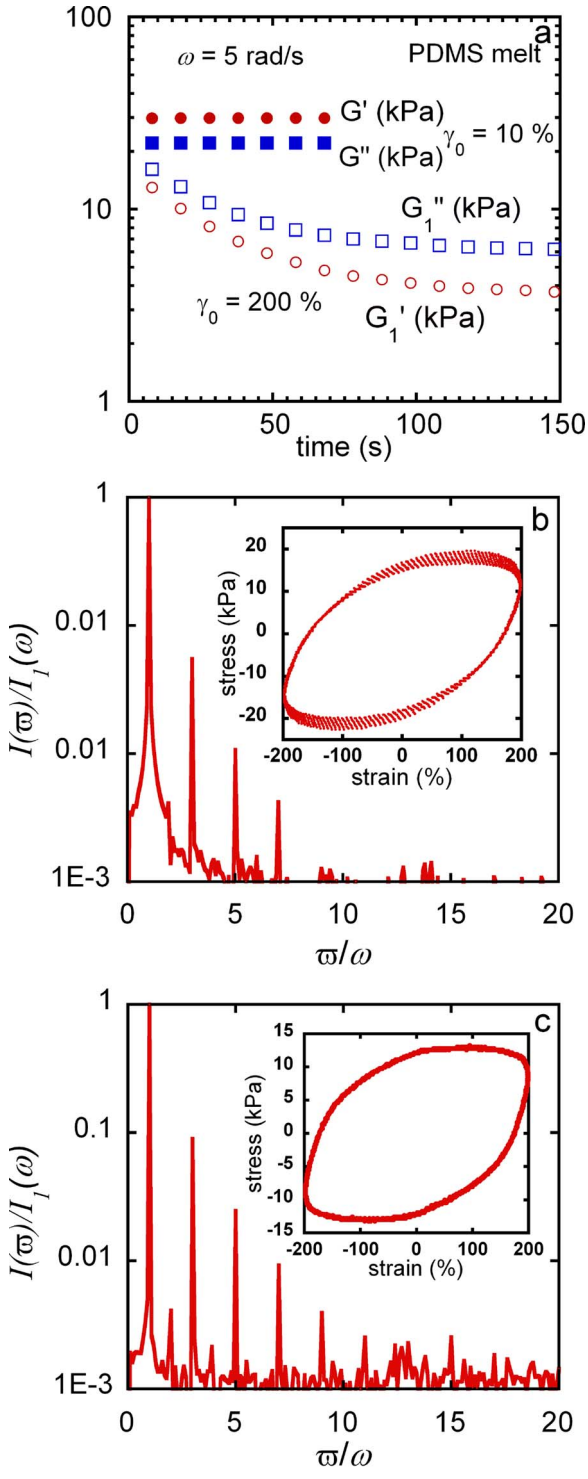

FIG. 13. (a) Time independence of G' and G'' at γ=10% (filled symbols) and decrease of G_1' and G_1'' at γ_0 =200% over time (open symbols), both at ω=5 rad/s measured in conventional cone-plate. (b) FT analysis of the shear stress around t=37 s with Lissajous loop involving several cycles. (c) FT analysis of the raw shear stress data along with the distorted Lissajous plot in steady state.

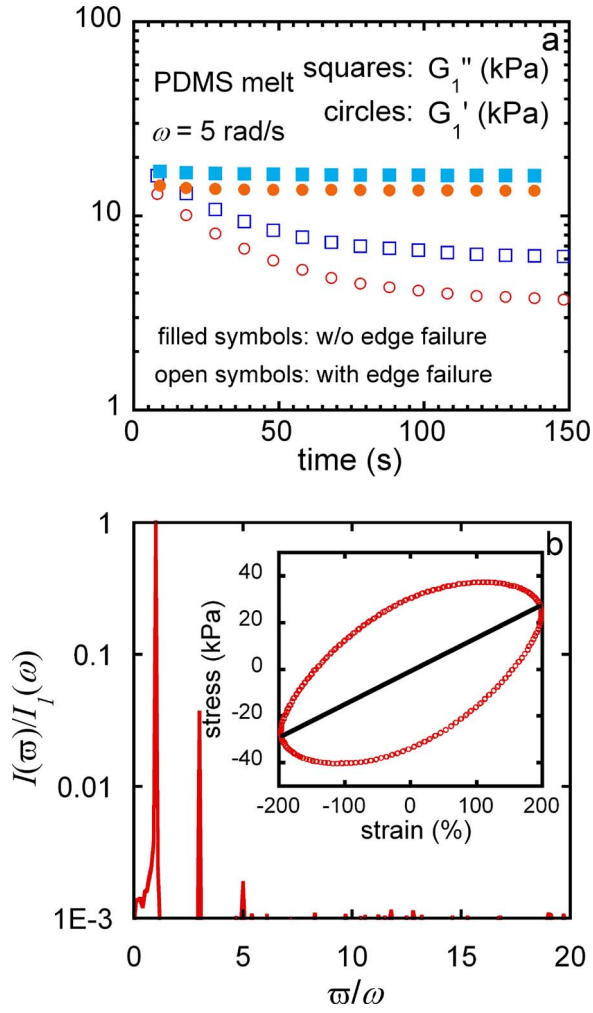

FIG. 14. (a) Time independence of G_1' and G_1'' (filled symbols) measured in the partitioned-plate-cone device in contrast to the decrease of G_1' and G_1'' (open symbols), both at $\gamma_0 = 200\%$ and $\omega = 5$ rad/s. (b) FT analysis of the shear stress in steady state corresponding to the filled symbols of (a), where the Lissajous loop is only slightly deviating from an ellipse.

sample allows the strain-induced yielding during LAOS to occur homogeneously. Unable to shear band due to the broad molecular weight distribution, the sample in steady state is also unable to significantly re-adjust its state of entanglement in each cycle. Consequently, the stress response is almost completely sinusoidal as shown in Fig. 14(b).

IV. CONCLUSIONS

Underlying microscopic structures of various viscoelastic materials tend to yield under large fast deformations such as LAOS. After the material is forced by LAOS to undergo a transition from elastic deformation to viscous flow, new states emerge. Such states may or may not be stable during LAOS. If the new state is stable then the shear stress response tends to be fairly sinusoidal in time. Conversely, if the system is able to switch from one state to another with in each cycle, strong wave distortion will be apparent in the stress

response. A common feature shared by all the present four systems is the significant strain softening under LAOS regardless of whether the final steady state displays appreciable wave distortion or not.

It is rare to have a viscoelastic system that would show linear response at large Deborah numbers during LAOS. The present study leaves the following questions unanswered. What experimental system is capable of exhibiting *nonlinearity* in LAOS without experiencing structural changes? How can stress response display significant non-sinusoidal time dependence without yielding or structural change within each cycle? Some associative materials studied by Ma *et al.* (1999) and Ewoldt *et al.* (2007) showed strain hardening within each cycle in steady state. It remains unclear whether the strain-hardening-like behavior was also due to structural changes (such as strain-induced association and dissociation) within each cycle.

Since yielding or structural disintegration in LAOS may not complete within the first oscillation cycle, one has to follow the process to steady state. For materials exhibiting time-dependent nonlinearity, it is difficult to identify any rheological fingerprint that would be analogous to G' and G'' for the equilibrium viscoelastic structure. We have examined four viscoelastic materials to illustrate a wide range of nonlinear behavior in LAOS. None of these four systems could greatly benefit from such treatments of the steady state as the FT analysis and the general stress decomposition method proposed by Cho *et al.* (2005) and improved by Ewoldt *et al.* (2008) and Yu *et al.* (2009). Specifically, we showed two examples (i.e., a nano-particle PBD melt and a polydisperse PDMS melt) of yielding in LAOS that involve little wave distortion and completely homogenous deformation, yet plenty of strain softening. We analyzed a familiar phenomenon of entangled PBD solution undergoing severe shear banding. We depicted a classical case of melt wall slip that does not produce even harmonics. Finally, we demonstrated how the commonly encountered edge fracture resulted in the production of even harmonics in both monodisperse PI melt and polydisperse PDMS melt during LAOS.

In summary, we reiterate the importance of identifying the time-dependent yielding process in LAOS of viscoelastic materials. Regardless of whether we can capture explicit evidence for yielding or not, it is perhaps inevitable to encounter structural change by LAOS in any viscoelastic liquids. The structural change induced by LAOS may not be generically depicted by classical constitutive (continuum mechanical) models, where the materials parameters are all constants with respect to both space and time. Thus, to theoretically quantify nonlinear LAOS of viscoelastic materials remains a formidable task. It seems that the first step toward depicting nonlinear LAOS behavior is to establish reliable phenomenology. Clearly, the steady-state character of LAOS is only a small window, through which we can peek into nonlinearity in LAOS. Homogeneous LAOS seems to imply sinusoidal response. Future study will determine whether there are exceptions to this statement. Conversely, it has yet to be demonstrated whether or not inhomogeneous LAOS necessarily results in wave distortion. Whether wave distortion occurs or not appears to depend essentially on whether the new microstructure is stable during each cycle of the LAOS.

ACKNOWLEDGMENT

This work is supported, in part, by a grant (Grant No. DMR-0821697) from the National Science Foundation.

References

Adrian, D. W., and A. J. Giacomin, "The quasi-periodic nature of a polyurethane melt in oscillatory shear," J. Rheol. **36**, 1227–1243 (1992).

Atalik, K., and R. Keunings, "On the occurrence of even harmonics in the shear stress response of viscoelastic fluids in large amplitude oscillatory shear," J. Non-Newtonian Fluid Mech. **122**, 107–116 (2004).

Boukany, P. E., and S. Q. Wang, "A correlation between velocity profile and molecular weight distribution in sheared entangled polymer solutions," J. Rheol. **51**, 217–233 (2007).

Boukany, P. E., and S. Q. Wang, "Exploring origins of interfacial yielding and wall slip in entangled linear melts during shear or after shear cessation," Macromolecules **42**, 2222–2228 (2009).

Boukany, P. E., S. Q. Wang, and X. R. Wang, "Step shear of entangled linear polymer: New experimental evidence for elastic yielding," Macromolecules (to be published).

Brochard, F., and P. G. de Gennes, "Shear-dependent slippage at a polymer/solid interface," Langmuir **8**, 3033–3037 (1992).

Cho, K. S., K. Hyun, K. H. Ahn, and S. J. Lee, "A geometrical interpretation of large amplitude oscillatory shear response," J. Rheol. **49**, 747–758 (2005).

Ewoldt, R. H., C. Clasen, A. E. Hosoi, and G. H. McKinley, "Rheological fingerprinting of gastropod pedal mucus and synthetic complex fluids for biomimicking adhesive locomotion," Soft Matter **3**, 634–643 (2007).

Ewoldt, R. H., A. E. Hosoi, and G. H. McKinley, "New measures for characterizing nonlinear viscoelasticity in large amplitude oscillatory shear," J. Rheol. **52**, 1427–1458 (2008).

Giacomin, A. J., and J. G. Oakley, "Structural network models for molten plastics evaluated in large-amplitude oscillatory shear," J. Rheol. **36**, 1529–1546 (1992).

Graham, M. D., "Wall slip and the nonlinear dynamics of large amplitude oscillatory shear flows," J. Rheol. **39**, 697–712 (1995).

Hatzikiriakos, S. G., and J. M. Dealy, "Wall slip of molten high-density polyethylene. 1. Sliding plate rheometer studies," J. Rheol. **35**, 497–523 (1991).

Jeyaseelan, R. S., and A. J. Giacomin, "Network theory for polymer solutions in large amplitude oscillatory shear," J. Non-Newtonian Fluid Mech. **148**, 24–32 (2008).

Klein, C. O., H. W. Spiess, A. Calin, C. Balan, and M. Wilhelm, "Separation of the nonlinear oscillatory response into a superposition of linear, strain hardening, strain softening, and wall slip response," Macromolecules **40**, 4250–4259 (2007).

Ma, L. L., J. Y. Xu, P. A. Coulombe, and D. Wirtz, "Keratin filament suspensions show unique micromechanical properties," J. Biol. Chem. **274**, 19145–19151 (1999).

Ravindranath, S., and S. Q. Wang, "What are the origins of stress relaxation behaviors in step shear entangled polymer solutions," Macromolecules **40**, 8031–8039 (2007).

Ravindranath, S., and S. Q. Wang, "Particle-tracking velocimetric investigation of large amplitude oscillatory shear behavior of entangled polymer solutions," J. Rheol. **52**, 341–358 (2008a).

Ravindranath, S., and S. Q. Wang, "Steady state measurements in stress plateau region of entangled polymer solutions: Controlled rate and controlled-stress modes," J. Rheol. **52**, 957–980 (2008b).

Reimers, M. J., and J. M. Dealy, "Sliding plate rheometer studies of concentrated polystyrene solutions: large amplitude oscillatory shear of a very high molecular weight polymer in diethyl phthalate," J. Rheol. **40**, 167–186 (1996).

Tapadia, P., and S. Q. Wang, "Direct visualization of continuous simple shear in non-Newtonian polymeric fluids," Phys. Rev. Lett. **96**, 016001 (2006).

Tapadia, P., S. Ravindranath, and S. Q. Wang, "Banding in entangled polymer fluids under oscillatory shearing," Phys. Rev. Lett. **96**, 196001 (2006).

Tee, T. T., and J. M. Dealy, "Nonlinear viscoelasticity of polymer melts," Trans. Soc. Rheol. **19**, 595–615 (1975).

Wang, S. Q., "Molecular transitions and dynamics at polymer/wall interfaces: Origins of flow instabilities and wall slip," Adv. Polym. Sci. **138**, 227–275 (1999).

Wang, S. Q., "A coherent description of nonlinear flow behavior of entangled polymers as related to processing

and numerical simulations," Macromol. Mater. Eng. **292**, 15–22 (2007).

Wang, S. Q., S. Ravindranath, P. Boukany, M. Olechnowicz, R. P. Quirk, A. Halasa, and J. Mays, "Nonquiescent relaxation in entangled polymer liquids after step shear," Phys. Rev. Lett. **97**, 187801 (2006).

Wang, X., J. E. Hall, S. Warren, J. Krom, J. M. Magistrelli, M. Rackaitis, and G. G. A. Bohm, "Synthesis, characterization, and application of novel polymeric nanoparticles," Macromolecules **40**, 499–508 (2007).

Wang, Y. Y., and S. Q. Wang, "Yielding during startup deformation of entangled linear polymeric liquids," J. Rheol. (to be published). Yielding associated with stress overshoot during startup deformation is rather evident: at high rates elastic recovery is 100% if the sample is let go before the force maximum is reached, which we call the yield point [see Ravindranath, S., and S. Q. Wang, "Universal scaling characteristics of stress overshoot in startup shear of entangled polymer solutions," J. Rheol. **52**, 681–695 (2008)], and Wang, Y., and S. Q. Wang, "From elastic deformation to terminal flow of a monodisperse entangled melt in uniaxial extension," *ibid.* **52**, 1275–1290 (2008)]. In the unpublished paper, yielding as a transition from elastic deformation to plastic flow is explored in terms of a microscopic picture. Yield is also commonly and appropriately used to refer to rheological behavior of yield-stress materials. There a yield-stress material exhibits largely elastic deformation until a threshold stress is exceeded to cause irrecoverable deformation, i.e., flow. In the present context of strain softening during LAOS, all four systems under study exhibit more liquid like behavior at high enough strains in contrast to their elastic characteristics observed at low strains in the linear response regime.

Wilhelm, M., "Fourier-transform rheology," Macromol. Mater. Eng. **287**, 83–105 (2002).

Wilhelm, M., D. Maring, and H. W. Spiess, "Fourier-transform rheology," Rheol. Acta **37**, 399–405 (1998).

Wilhelm, M., P. Reinheimer, and M. Ortseifer, "High sensitive Fourier-transform rheology," Rheol. Acta **38**, 349–356 (1999).

Yu, W., P. Wang, and C. X. Zhou, "General stress decomposition in nonlinear oscillatory shear flow," J. Rheol. **53**, 215–238 (2009).

Zhu, Z. Y., T. Thompson, S. Q. Wang, E. D. von Meerwall, and A. Halasa, "Investigating linear and nonlinear viscoelastic behavior using model silica-particle-filled polybutadiene," Macromolecules **38**, 8816–8824 (2005).